Dynamic and Thermodynamic Properties of Porous Vortex Matter in Bi$_2$Sr$_2$CaCu$_2$O$_8$ in an Oblique Magnetic Field

Nurit Avraham,[1] Y. Y. Goldschmidt,[2] J. T. Liu,[2] Y. Myasoedov,[1] M. Rappaport,[1] E. Zeldov,[1] C. J. van der Beek,[3]
M. Konczykowski,[3] and T. Tamegai[4]

[1]*Department of Condensed Matter Physics, The Weizmann Institute of Science, Rehovot 76100, Israel*
[2]*Department of Physics and Astronomy, University of Pittsburgh, Pittsburgh, Pennsylvania 15260, USA*
[3]*Laboratoire des Solides Irradiés, CNRS UMR 7642 and CEA-CMS-DRECAM, Ecole Polytechnique, 91128 Palaiseau, France*
[4]*Department of Applied Physics, The University of Tokyo, Hongo, Bunkyo-ku, Tokyo 113-8656, Japan*

Vortex matter in Bi$_2$Sr$_2$CaCu$_2$O$_8$ with a low concentration of tilted columnar defects (CDs) was studied using magneto-optical measurements and molecular dynamics simulations. It is found that while the dynamic properties are significantly affected by tilting the magnetic field away from the CDs, the thermodynamic transitions are angle independent. The simulations indicate that vortex pancakes remain localized on the CDs even at large tilting angles. This preserves the vortex thermodynamics, while vortex pinning is considerably weakened due to kink sliding.

The dynamic and thermodynamic properties of vortex matter in high T_c superconductors are strongly affected by the introduction of columnar defects (CDs). In the presence of a low concentration of CDs, experimental [1–3] and theoretical results [4–9] indicate the presence of two vortex subsystems: vortices localized on pinning centers and interstitial vortices between them. At low temperature, a *porous vortex solid* phase is created. A rigid matrix of vortices, strongly pinned on a network of random CDs, is formed, while the interstitial vortices create relatively ordered nanocrystals within the pores of the matrix. When the temperature is increased, the interstitial vortices melt while the rigid matrix remains localized, forming a *nanoliquid* phase in which nanodroplets of liquid are weakly confined within the pores of the matrix. When temperature is increased further, the matrix delocalizes at the delocalization transition, and the liquid becomes *homogeneous*.

This picture holds when the angle θ between the average induction **B** and the CDs is zero. According to theoretical models [10,11], for small θ, the localized vortices on CDs remain completely trapped along the CDs. At larger θ, the vortices form a staircase structure while at still larger angles, the vortices follow the field direction and are not affected by the correlated nature of the CDs. In general, one expects the effect of the correlated nature of the CDs to decrease as θ increases and to vanish at $\theta = 90°$. In more isotropic materials such as YBa$_2$Cu$_3$O$_7$, this picture is supported by various experiments, showing an angle dependent behavior in both dynamic [12] and thermodynamic [13] properties. In layered materials such as Bi$_2$Sr$_2$CaCu$_2$O$_8$ (BSCCO), vortices consist of stacks of two-dimensional pancake vortices (PVs) defined in the CuO$_2$ layers only. Measurements of the equilibrium torque and magnetization in BSCCO [14] have shown that the CD occupation by PVs in the liquid phase is angle indepen-

dent. In contrast, Josephson plasma resonance measurements [15] show that the PV alignment in the liquid is significantly affected by CDs. The corresponding equilibrium properties of the solid phase have not been studied. Since the melting transition depends on the difference in the behavior of the free energies of the solid and liquid, it is very interesting to study the angular dependence of the melting in the presence of CDs. Moreover, CDs are known to shift the melting line upward [1] and point disorder was found to shift it downward [16]. One might expect, therefore, that tilting **B** away from the CDs would shift the melting line continuously from above the pristine melting line to below it.

Here, we study the angular dependence of the dynamic and thermodynamic properties of porous vortex matter in BSCCO. Our measurements show that the irreversibility line shifts to lower T when the field is tilted away from the CDs, as expected [12,17]. However, the thermodynamic melting and delocalization lines have *no* angular dependence. Our simulations show that even at large angles the PVs are effectively pinned by the CDs and therefore the thermodynamic features remain unaffected. On the other hand, the formation of a kink structure of the PV stacks increases their mobility due to kink sliding, therefore suppressing the irreversible properties.

For the measurements, BSCCO crystals ($T_c \approx 90$ K) were irradiated, at GANIL, with 1 GeV Pb ions, through stainless steel masks with triangular arrays of 90 μm holes. This results in the formation of columnar tracks, with density n_d equal to the ion dose, in the holes only. Crystals A and B, irradiated at 45° with respect to the c axis, have matching fields $B_\phi = n_d\Phi_0$ of 20 G and 30 G, respectively. The measurements were performed using differential magneto-optical imaging (DMO) [18] with a vector magnet that allows application of a dc magnetic field in any direction, so that the local magnetic response

can be imaged over the full range of angles from **B** ∥ CDs
($\theta = 0$) to **B** ⊥ CDs ($\theta = 90°$).

Figure 1(a) shows the irreversibility line of the irradiated
regions $H_{irr}^{cd}(T)$ on an $H_z - T$ plane, where H_z is the c-axis
component of the applied field, for different angles of **B**
with respect to the CDs. The curves were obtained using
DMO with field modulation of 1 Oe, upon sweeping the
temperature. Below $H_{irr}^{cd}(T)$, the external field modulation
is shielded in the irradiated regions due to enhanced pin-
ning [1]. Hence, the dark regions in the DMO image
[Fig. 1(b)] are the irradiated regions, while the bright
background is the reversible pristine region. Upon increas-
ing T, these dark regions gradually fade until they disap-
pear completely at $H_{irr}^{cd}(T)$, where the screening current
drops to an unobservably low level.

Figure 1(a) shows that upon tilting the field away from
the CDs (changing θ from 0 to 90°), the irreversibility line
shifts to lower temperatures. For example, at $H_z = 70$ Oe
the irreversibility temperature at 90° is 2.5 K lower than at
$\theta = 0$. Even at $\theta = 90°$, $H_{irr}^{cd}(T)$ remains slightly above the
melting line of the vortex lattice in the pristine crystal,
$H_m^p(T)$. This is at odds with the expectation that at $\theta = 90°$
the CDs act as weak point disorder; then, the melting and
irreversibility lines are expected to lie below $H_m^p(T)$ [16].
The angular dependence of $H_{irr}^{cd}(T)$ is more pronounced at
lower temperatures. It decreases upon increasing T until it
disappears at ~82 K, above which all lines coincide with
$H_m^p(T)$. This behavior was observed for different samples
with B_ϕ of 20, 30, and 40 G. The relative shift in $H_{irr}^{cd}(T)$
between $\theta = 0$ to 90° was found to increase with B_ϕ.

To examine the vortex behavior below $H_{irr}^{cd}(T)$, within
the vortex solid phase, we performed conventional MO
measurements, in which a sequence of images is taken
while the applied field H_a is swept. Figure 1(c) shows
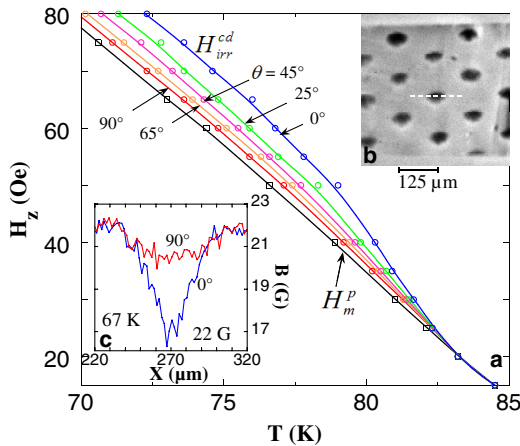flux profiles across the irradiated regions. These have a

linear (Bean-like) shape due to the enhanced pinning in
these regions. The profiles were taken at $H_z = 22$ Oe and
$T = 67$ K, well below $H_{irr}^{cd}(T)$. At $\theta = 90°$, the profile is
very shallow. In contrast, at $\theta = 0$, a clear sharp profile is
observed. The critical current, estimated from the flux
gradient, is 3.5 times higher at $\theta = 0$ than at 90°.

The angular dependence of the melting transition was
studied using DMO upon temperature sweeps with T
modulation [1,18]. The first-order melting transition is
characterized by a step in the equilibrium flux density,
and it appears as a bright signal in the DMO images. For
example, the bright circular regions in Fig. 2(a) are the
irradiated areas that undergo melting, while the surround-
ing pristine regions are already in the liquid phase and
hence appear as a darker background.

Figure 2(b) shows the local DMO intensity, averaged
over a region of 15×15 μm^2 in one of the irradiated
regions [red square in Fig. 2(a)]. The melting transition
manifests itself as a peak in the local intensity as T is
swept. Each curve corresponds to a different θ, while $H_z =
35$ Oe was kept constant. In contrast to the irreversibility
line that shifts to lower T upon increasing θ, the melting
temperature remains unaffected, even when **B** is perpen-
dicular to the CDs. Moreover, the transition width, deter-
mined from the width of the peak, appears to be the same
for all measured angles. Similar results were obtained for
different H_z values. Note that the pristine melting line was
found to have a weak linear dependence on the in-plane
field [19] which cannot be detected within our experimen-
tal resolution for our low in-plane fields.

Figure 3(a) gathers the melting lines obtained at differ-
ent angles θ. They all fall on a single line, $H_m^{cd}(T)$, that
terminates at a critical point (CP) below which the tran-
sition becomes continuous in nature. The CP occurs at the
same temperature of 77 K at all angles. The width of the
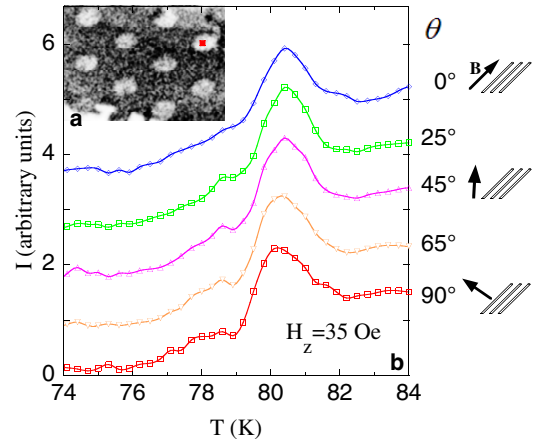transition, denoted by the horizontal right-pointing arrows,

FIG. 1 (color online). (a) The irreversibility line $H_{irr}^{cd}(T)$ of
crystal A, mapped for five angles θ between **B** and the CDs,
from $\theta = 0$ to 90°. H_m^p is the pristine melting line. (b) DMO
image of part of the sample at $T = 79$ K and $H_z = 35$ Oe.
(c) Flux profiles across the irradiated region [dashed line in
(b)], at 67 K and $H_z = 22$ Oe, for $\theta = 0°$ and 90°.

FIG. 2 (color online). The melting transition in crystal B.
(a) DMO image of part of the sample at $H_z = 35$ Oe, $T =
81$ K. (b) Local DMO intensity vs T for different angles θ.
The peak around 80.4 K corresponds to the melting transition.
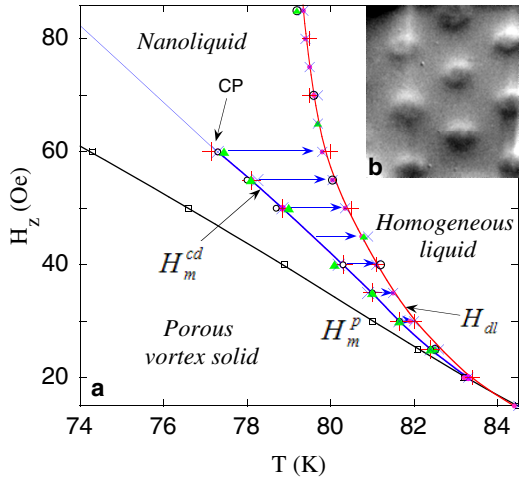The curves are vertically displaced for clarity.

FIG. 3 (color online).   (a) The melting line $H_m^{cd}(T)$ and the delocalization line $H_{dl}(T)$ in crystal A, mapped for different θ: $0(+)$, $25°(\bigcirc)$, $45°(\bullet)$, $65°(\blacktriangle)$, and $90°(\times)$. (b) DMO self-field image of part of sample A at 40 Oe, 75 K, 20 mA.

is broadened on approaching the CP, but remains independent of angle, as was already shown in Fig. 2 for $H_z =$ 35 Oe. In Fig. 3, we also plot the delocalization line $H_{dl}(T)$ [2], which separates the nanoliquid from the homogeneous liquid. $H_{dl}(T)$ was determined using MO visualization of the self-field induced by a transport current applied to the sample. DMO image of the self-field allows one to visualize the transport current density distribution within the sample. Below $H_{dl}(T)$, the current flow is highly nonuniform due to enhanced pinning in the irradiated regions [2], and the DMO image shows significant spatial variations [Fig. 3(b)]. These disappear at H_{dl}, when the network of pinned vortices is delocalized, and a homogeneous liquid is formed. As $H_m^{cd}(T)$, the $H_{dl}(T)$ does not depend on the field angle θ. On approaching T_c, vortex pinning by CDs becomes weak and hence all the transition lines coincide.

The experimental observations show that the dynamic properties of porous vortex matter are strongly dependent on the angle between **B** and the CDs, while the thermodynamic melting and delocalization lines are angle independent. In order to understand these observations, we have carried out molecular dynamics simulations of a rectangular parallelepiped model system of 36 PV stacks and 200 layers. As shown in [9,20], such a system size is sufficient for observing the various phase transitions. Periodic boundary conditions (PBC) were implemented in all directions. The intraplane PV interaction was modeled by the repulsion of their screening currents, while the interplane PV interaction is described by their mutual electromagnetic attraction. For details, see Refs. [9,21]. We also included the attractive Josephson interaction between pairs of pancakes in adjacent planes, but belonging to the same stack [21]. We keep track of pancakes belonging to a vortex stack and allow for flux cutting and recombination [21]. The average vortex direction (i.e., H_a) was kept parallel to the z axis, while tilted CDs of radius $r_r = 30$ nm were

introduced at random positions. The interaction between a pancake and a CD in the same plane is given by an attractive potential [9,11], which has a long range tail contribution $\approx -\epsilon_0 d r_r^2/R^2$, due mainly to the electromagnetic pinning, and a short range flat region of depth $\approx \epsilon_0 d$ due to the combined effects of electromagnetic and core pinning. Here, $\epsilon_0 = (\phi_0/4\pi\lambda)^2$, $\lambda = \lambda(0)/(1 - T/T_c)^{1/2}$ is the penetration depth, R is the distance between a pancake and a CD, and d is the layer separation. The interaction $-\mathbf{B} \cdot \mathbf{H}/(4\pi)$ is implemented by the PBC, since the electromagnetic interaction between a tilted stack and the stacks of images, positioned above (and below) its center of mass, pull the tilted stack in the z direction. Temperature effects are implemented in the simulation by using a white thermal noise whose variance is proportional to the temperature.

Figure 4 shows projections of the vortices onto the xy plane (top view) and the xz plane (side view), with CDs tilted by 45° and 80°. The main observation is that, for $B > B_\phi$, the CDs are almost fully decorated by pancakes both in the solid and nanoliquid phases. This means that the matrix of pinned PVs is preserved even when the field is tilted away from the CDs, and as a result the interstitial PVs remain caged in the surrounding fixed matrix. The interstitial PV stacks are even found to be tilted to some extent in the direction of CDs, in the solid phase. Another important observation is that the vortices adopt a structure featuring kinks between the layers, as shown by the side views in Figs. 4(c) and 4(d). Kinks of different vortices tend to align, forming a structure which resembles the
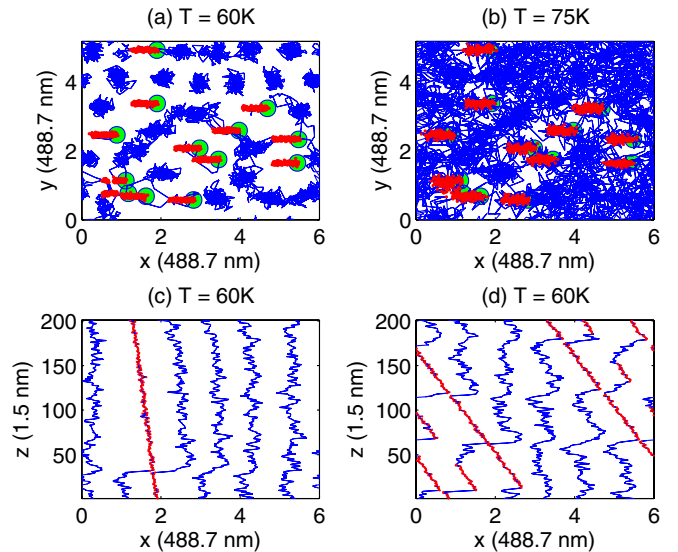

FIG. 4 (color online).   Snapshots of vortex stacks and CDs tilted at 45° (a)–(c) and 80° (d) for $B = 100$ G and $B_\phi^{eff} = 35$ G. Pancakes in the same stack are connected. Free pancakes are in blue, trapped ones in red. Only CDs at the bottom layer are shown (green). (a), (b) Projection onto the a-b plane (top view). (a) Nanosolid phase. (b) Nanoliquid phase. (c) Projection of (a) onto the a-c plane (side view), first row is shown. (d) Side view with CDs at 80°.

Josephson and Abrikosov crossing lattices [22] in BSCCO at tilted field. Here, however, the Josephson vortices (JV) are formed when tilting the field away from CDs rather than from the c axis.

To further interpret the results we consider the energies involved: the binding energy of a vortex to a CD is of the order of $\epsilon_0 d$ per layer. For angles less than about 75° this gain exceeds the electromagnetic energy loss. For an infinitely long stack tilted at angle θ, the latter is given by $\epsilon_0 d \ln\{[1 + \cos(\theta)]/2\cos(\theta)\}$ per layer [23]. In addition, the energy $-\mathbf{B} \cdot \mathbf{H}/(4\pi)$ tends to align the average vortex orientation with $\mathbf{H}$. The contradicting requirements imposed by the need to minimize the total energy are met by the creation of kinks. The Josephson energy cost of the kinks is negligible compared to the total energy of the vortex system in a highly anisotropic material like BSCCO [24]. Indeed, for $\gamma \sim 375$, the total energy measured in the simulations for nontilted CDs and for CDs tilted at 45° is the same, in the vicinity of the melting transition ($T = 73$ K to 77 K), within the simulation's error bars. The comparison was done for the same value of $B_\phi^{\text{eff}} = B_\phi \cos\theta$ in order to match the experimental situation where the ratio of vortices to CDs remains fixed as θ changes. Our simulations show that the rigid matrix of pancakes pinned on CDs is preserved up to very large angles in both the solid and nanoliquid vortex phases. This means that the enhanced caging potential created by the CDs that was found to shift the melting line upwards [1] is negligibly affected by increasing the angle between $\mathbf{B}$ and the CDs. Consequently, the thermodynamic properties, in particular, the melting and delocalization lines, are angle independent. This was verified in our simulations for $B = 100$ G, where the melting and delocalization transitions occur at 74 K and 76 K, respectively, both for nontilted and tilted CDs, as evidenced by measurements of the mean square deviation of the flux lines, the amount of their entanglement, and other measurements [25].

These observations can resolve the apparent discrepancy between the dynamic and thermodynamic properties. The kinks developed by the vortices have a negligible effect on the thermodynamics but a large effect on the dynamics. As demonstrated by our simulations, the kinks slide along the CDs due to the Lorentz force exerted by in-plane current [10,26]. Consequently, they transfer PVs between segments, thus producing an effective transverse drift of the whole pancake stack. Upon increasing θ, the amount of kinks increases and the flux creep becomes more effective. This process decreases the critical current and shifts the irreversibility line to lower temperatures. This is consistent with [14], which concluded that CDs' pinning anisotropy commonly measured in BSCCO [17] must be a dynamic effect.

In summary, the porous vortex matter in BSCCO is shown to preserve its thermodynamic properties even when the field is tilted away from the CDs. While the irreversibility line shifts to lower temperatures upon tilting the field, the thermodynamic melting and delocalization lines remain constant. Numerical simulation shows that increasing the angle between the field and the CDs leads to formation of weakly pinned vortex kinks, while preserving the basic structure of a rigid matrix of pancake stacks residing along the CDs with nanocrystals of interstitial vortices embedded within the pores of the matrix.

[1] S. S. Banerjee *et al.*, Phys. Rev. Lett. **90**, 087004 (2003).
[2] S. S. Banerjee *et al.*, Phys. Rev. Lett. **93**, 097002 (2004).
[3] M. Menghini *et al.*, Phys. Rev. Lett. **90**, 147001 (2003).
[4] L. Radzihovsky, Phys. Rev. Lett. **74**, 4923 (1995).
[5] S. Tyagi and Y. Y. Goldschmidt, Phys. Rev. B **67**, 214501 (2003).
[6] C. Dasgupta *et al.*, Phys. Rev. Lett. **91**, 127002 (2003).
[7] Y. Nonomura and X. Hu, Europhys. Lett. **65**, 533 (2004).
[8] A. V. Lopatin and V. M. Vinokur, Phys. Rev. Lett. **92**, 067008 (2004).
[9] Y. Y. Goldschmidt and E. Cuansing, Phys. Rev. Lett. **95**, 177004 (2005).
[10] D. R. Nelson and V. M. Vinokur, Phys. Rev. B **48**, 13 060 (1993).
[11] G. Blatter *et al.*, Rev. Mod. Phys. **66**, 1125 (1994).
[12] L. Civale *et al.*, Phys. Rev. Lett. **67**, 648 (1991); A. Silhanek *et al.*, Phys. Rev. B **59**, 13 620 (1999).
[13] B. Hayani *et al.*, Phys. Rev. B **61**, 717 (2000).
[14] R. J. Drost *et al.*, Phys. Rev. B **58**, R615 (1998).
[15] N. Kameda *et al.*, Phys. Rev. B **72**, 064501 (2005).
[16] B. Khaykovich *et al.*, Phys. Rev. B **56**, R517 (1997).
[17] C. J. van der Beek *et al.*, Phys. Rev. Lett. **74**, 1214 (1995); W. S. Seow *et al.*, Phys. Rev. B **53**, 14 611 (1996); V. Hardy *et al.*, Phys. Rev. B **54**, 656 (1996).
[18] A. Soibel *et al.*, Nature (London) **406**, 282 (2000).
[19] B. Schmidt *et al.*, Phys. Rev. B **55**, R8705 (1997); S. Ooi *et al.*, Phys. Rev. Lett. **82**, 4308 (1999).
[20] H. Nordborg and G. Blatter, Phys. Rev. B **58**, 14 556 (1998).
[21] S. Tyagi and Y. Y. Goldschmidt, Phys. Rev. B **70**, 024501 (2004); Y. Y. Goldschmidt, Phys. Rev. B **72**, 064518 (2005); Y. Y. Goldschmidt and S. Tyagi, Phys. Rev. B **71**, 014503 (2005).
[22] A. E. Koshelev, Phys. Rev. Lett. **83**, 187 (1999).
[23] J. R. Clem, Phys. Rev. B **43**, 7837 (1991).
[24] L. N. Bulaevskii *et al.*, Phys. Rev. Lett. **77**, 936 (1996).
[25] Y. Y. Goldschmidt and J. T. Liu (to be published).
[26] D. R. Nelson and V. M. Vinokur, Phys. Rev. Lett. **68**, 2398 (1992); M. V. Indenbom *et al.*, Phys. Rev. Lett. **84**, 1792 (2000).